Editors' Suggestion

Local signatures of altermagnetism

Jannik Gondolf,[1] Andreas Kreisel,[1] Mercè Roig,[1,2] Yue Yu,[2] Daniel F. Agterberg,[2] and Brian M. Andersen[1]
[1]*Niels Bohr Institute, University of Copenhagen, DK-2200 Copenhagen, Denmark*
[2]*Department of Physics, University of Wisconsin-Milwaukee, Milwaukee, Wisconsin 53201, USA*

(Received 26 February 2025; accepted 5 May 2025; published 21 May 2025)

Altermagnets constitute a class of collinear compensated Néel ordered magnets that break time-reversal symmetry and feature spin-split band structures. Based on versatile microscopic models able to capture the altermagnetic sublattice degrees of freedom, we study characteristic local signatures of altermagnetism near disorder sites. We give a complete list of two-dimensional models that exhibit altermagnetism classified by their corresponding layer groups. Specifically, we calculate the local density of states in the vicinity of pointlike nonmagnetic impurities and expose its spatial dependence for two minimal models showcasing d-wave and g-wave altermagnetism. The momentum structure of the nodes (d-wave, g-wave, etc.) is directly imprinted on the total local density of states, thus measurable by scanning tunneling conductance experiments. This signature is present both in the spin-resolved as well as the spin-summed local density of states. We find a weaker response in the nonmagnetic state from the anisotropic crystal environment and uncover the importance of the sublattice degree of freedom to model altermagnets. We also study coexistence phases of altermagnetism and superconductivity and provide predictions for the local impurity response of in-gap bound states. The response of impurity bound states strongly enhances the distinct altermagnetic signature.

DOI: 10.1103/PhysRevB.111.174436

I. INTRODUCTION

Altermagnets have been identified as a distinct class of collinear compensated magnetic order in addition to standard antiferromagnetism [1,2]. As opposed to conventional antiferromagnets, Néel ordered altermagnets lack inversion or translation together with time reversal as a combined symmetry, but exhibit instead time reversal and a rotation (proper or improper) as a combined symmetry of the magnetic state. This distinction can originate from anisotropic local crystal environments around the different sublattice sites. Thus the Néel order of altermagnets exhibits the same unit cell as the original normal state. The unique properties of altermagnets have profound implications for their electronic properties, most notably the existence of large momentum-dependent spin-split electronic bands, even in the absence of relativistic spin-orbit coupling. Spin splitting has recently been detected by angular-resolved photoemission spectroscopy (ARPES) on a number of altermagnetic candidate materials, for example, CrSb [3,4], MnTe [5–7], and RuO_2 [8]. The altermagnetic spin-split bands that arise in a material with negligible net magnetization and absence of harmful stray fields have led to the proposal of several applications of altermagnetism within spintronics [1,9]. However, a fundamental challenge is the presence of domains that may limit their applicability and complicate the experimental interpretation of the unique signatures of altermagnets. The latter motivates studies of local signatures of altermagnetic order. What should local atomic-scale resolved probes detect as characteristic features of altermagnetic order? From studies of the local impurity response in unconventional superconductors, for example, it is well known that impurities can provide useful information on the fundamental properties of the host [10–15].

Here we address the question of local signatures of altermagnetic order, starting from recently developed microscopic minimal Hamiltonian models for altermagnets. The framework developed in Ref. [16] provided 40 electronic models for all centrosymmetric space groups with magnetic atoms occupying inversion-symmetric Wyckoff positions of multiplicity two. This includes monoclinic, orthorhombic, tetragonal, rhombohedral, hexagonal, and cubic materials and describes d-wave, g-wave, and i-wave altermagnetism [16]. Thus the minimal models are general, yet may also become material specific through parameter constraints from density functional theory (DFT) or experiments and respect all symmetries of the crystal in the normal state and the altermagnetic state. Clearly, a significant advantage of having such minimal models is the ability to perform analytical calculations and derive general formulas that apply to broad classes of altermagnetic materials. Examples of this approach are found in Refs. [16,17], where general expressions for the Berry curvature are reported, allowing for calculations of the anomalous Hall effect (AHE), resulting in the insight that altermagnets exhibit AHE linear in their spin-orbit coupling. Other recent examples of the usefulness of microscopic minimal models include derivations of connections between quantum geometry and altermagnetic instabilities [18] and studies of altermagnetic antichiral surface states and domain wall bound states [19].

In this work, we apply microscopic minimal Hamiltonian models for altermagnetism to obtain the local Green's function near disorder sites. For concreteness and simplicity, we focus on minimal models that can be obtained from three-dimensional (3D) tight-binding models as presented in Ref. [16] by removing the k_z dependence. These models belong to space groups 11, 13, 14, 51, 55, 83, 123, and 127 and

have either d-wave or g-wave spin-split bands. In Appendix B, we give the corresponding 2D models as classified by the corresponding 2D layer groups. As deduced from Table II, the models considered in this work are relevant for layer groups L17, L44, L63 and, in a special case, to L51. For a high-throughput computational search of 2D altermagnetic candidate materials, we refer to Ref. [20], which includes a series of 2D candidates for which our models apply. We stress, however, that the results of local signatures of altermagnetic order obtained below may also apply to 3D altermagnets, depending on their particular surface termination. In order to address the impurity problem, we apply both a T-matrix formulation and perform real-space self-consistent calculations to determine the local density of states (LDOS) response near pointlike impurities. We find that the altermagnetic characteristics are directly imprinted on the total LDOS, allowing for detection of local altermagnetism and its associated momentum structure. Finally, we also discuss the impurity properties of altermagnets coexisting with superconductivity. In this case, in-gap impurity bound states are generated by both magnetic and nonmagnetic pointlike impurities. The bound state wave function features clear signatures of the underlying altermagnetic order.

Some earlier work has addressed local markers for altermagnetic order, including bound states near lattice dislocations [21], spin-polarized subgap states in altermagnetic superconductors [22], and characteristics of impurity-induced Friedel oscillations in altermagnetic metals [23–25]. Here, we focus on the role of pointlike nonmagnetic impurities. As shown below, our results are qualitatively different from those presented in Refs. [22–25]. The important distinction originates from the applied minimal model used to describe altermagnetic materials. Whereas the results in Refs. [22–25] were based on a one-band model with momentum-dependent spin splitting, our minimal models for altermagnetism are based on fundamental symmetries, i. e., the relationship between the site symmetry of magnetic atoms and the point group symmetry of the space group [16]. As a consequence, such minimal models incorporate the (lower) symmetry already in the nonmagnetic normal state. Indeed, in the minimal models we consider here, the instability into the altermagnetic state is driven by antiferromagnetism and the altermagnetic spin spitting is an induced order parameter. In single band models of Refs. [22–25], the altermagnetic spin splitting is the primary order parameter. The main distinction between the results of the impurity response of the two approaches is whether local anisotropies exist in the total LDOS or only in the spin-resolved LDOS. We find that the total LDOS exhibits direct local signatures of the altermagnetic order, whereas the one-band models feature such signatures only in the spin-resolved impurity response.

The paper is organized as follows. In Sec. II we introduce the basic methodology, including both the T-matrix formalism of a single impurity and the self-consistent real-space formulation of the problem. Section III presents our main results for total and spin-resolved LDOS near pointlike disorder sites in both d-wave and g-wave altermagnets. Altermagnetic symmetries are directly imprinted onto the LDOS near impurities. In Secs. III C and III D we contrast the results to those obtained within a single-band model and in Sec. III E we discuss potential interplay with superconductivity. Finally, Sec. IV contains our conclusions.

II. METHODOLOGY

Throughout this study we begin with the minimal model for altermagnets derived in Ref. [16]

$$\mathcal{H}_{\mathrm{MM}} = \varepsilon_{0,\mathbf{k}}\tau_0 + t_{x,\mathbf{k}}\tau_x + t_{z,\mathbf{k}}\tau_z + \tau_y\vec{\lambda}_{\mathbf{k}}\cdot\vec{\sigma} + \tau_z\vec{N}\cdot\vec{\sigma}, \quad (1)$$

where σ_i and τ_i are the Pauli matrices for the spin and sublattice degrees of freedom, respectively. The energy dispersion $\varepsilon_{0,\mathbf{k}}$ is independent of the sublattice and $t_{x,\mathbf{k}}$ and $t_{z,\mathbf{k}}$ denote inter- and intrasublattice hoppings, respectively. The crystal asymmetric hopping $t_{z,\mathbf{k}}$ describes the local symmetry breaking already in the normal state, as it transforms as a nontrivial irreducible representation of the point group. Neglecting spin-orbit coupling given by the term $\vec{\lambda}_{\mathbf{k}}$, the quantization axis of the Néel order parameter N can be chosen along the z direction. To make Fourier transformations simpler and restrict k-space integrations to the first Brillouin zone (BZ) only, we perform a gauge transformation of the B sublattice creation and annihilation operators as $c_{\sigma B,\mathbf{k}} \to c_{\sigma B,\mathbf{k}}e^{i\phi_{\mathbf{k}}}$. In the new basis, $t_{x,\mathbf{k}} \to t_{x,\mathbf{k}}e^{i\phi_{\mathbf{k}}}$ such that the Hamiltonian exhibits the full periodicity of the BZ for $\phi_{\mathbf{k}} = -\frac{k_x}{2} - \frac{k_y}{2}$. The minimal model then reads

$$\mathcal{H} = \varepsilon_{0,\mathbf{k}}\tau_0 + t_{z,\mathbf{k}}\tau_z + \mathrm{Re}[t_{x,\mathbf{k}}]\tau_x - \mathrm{Im}[t_{x,\mathbf{k}}]\tau_y + N\tau_z\sigma_z. \quad (2)$$

The explicit momentum dependence of all expressions and tight-binding parameters are given in Appendix A. Note that $\mathcal{H}$ is block diagonal in the spin index σ and each block can be diagonalized as $U^{\dagger}_{\sigma,\mathbf{k}}\mathcal{H}_{\sigma}U_{\sigma,\mathbf{k}} = \mathrm{diag}(E^{+}_{\sigma,\mathbf{k}}, E^{-}_{\sigma,\mathbf{k}})$ with eigenvalues $E^{\beta}_{\sigma,\mathbf{k}} = \varepsilon_{0,\mathbf{k}} + \beta\sqrt{|t_{x,\mathbf{k}}|^2 + (t_{z,\mathbf{k}} + \sigma N)^2}$ and unitary transformation

$$U_{\sigma,\mathbf{k}} = \begin{pmatrix} \cos\frac{\theta_{\sigma,\mathbf{k}}}{2} & \frac{t_x}{|t_x|}\sin\frac{\theta_{\sigma,\mathbf{k}}}{2} \\ -\frac{t_x^*}{|t_x|}\sin\frac{\theta_{\sigma,\mathbf{k}}}{2} & \cos\frac{\theta_{\sigma,\mathbf{k}}}{2} \end{pmatrix}, \quad (3)$$

where

$$\cos\frac{\theta_{\sigma,\mathbf{k}}}{2} = \frac{1}{\sqrt{2}}\sqrt{1 + \frac{t_z + \sigma N}{\sqrt{|t_x|^2 + (t_z + \sigma N)^2}}}, \quad (4)$$

$$\sin\frac{\theta_{\sigma,\mathbf{k}}}{2} = \frac{-1}{\sqrt{2}}\sqrt{1 - \frac{t_z + \sigma N}{\sqrt{|t_x|^2 + (t_z + \sigma N)^2}}}, \quad (5)$$

and $\beta \in \{-1, 1\}$ is a band index. Figure 1 shows an exemplary d-wave altermagnet. The anisotropic crystal environments and hoppings for the sublattices are shown in Fig. 1(a). The spin-split Fermi surface and band structure can be seen in Figs. 1(b)–1(f), also showing the sublattice mixing but pure spin character of the bands.

A. T-matrix formalism

To study local signatures of altermagnetic order close to impurities, we employ the T-matrix framework. We consider scattering with strength V_{imp} on a nonmagnetic on-site impurity potential in the elementary cell at the

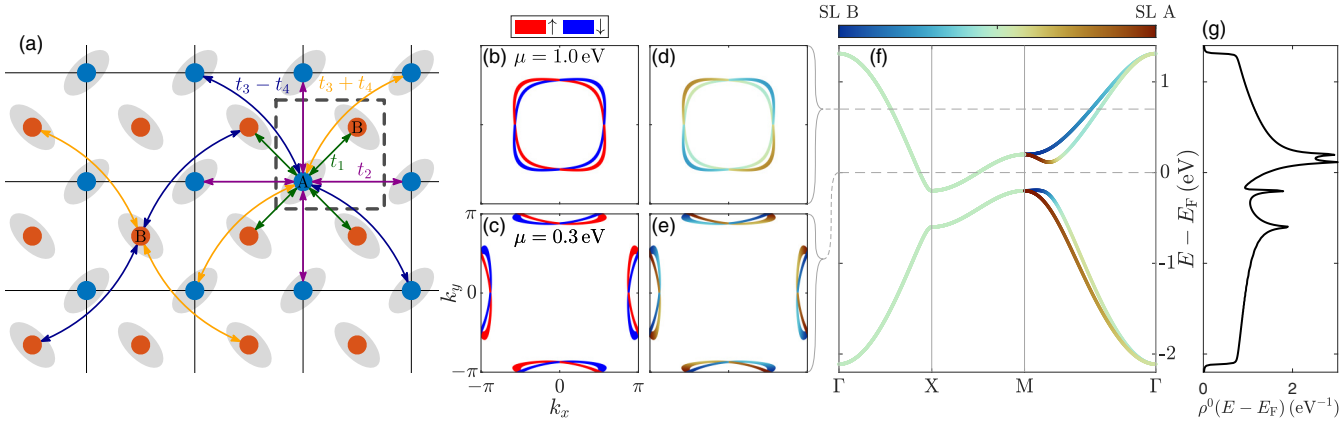

FIG. 1. (a) Sketch of the crystal lattice and the hopping parameters representing layer group 63 with lattice sites at Wyckoff position 2*b*. The unit cell is indicated by the dashed box. The hopping term responsible for altermagnetism $t_z \propto t_4$ has opposite signs for sublattices *A* and *B* and breaks C_4 symmetry [16]. The sublattices are related by translation combined with rotation by 90° due to the anisotropic nonmagnetic environment indicated by gray ellipses. (b), (c) Fermi surface for $\mu = 1$ eV and $\mu = 0.3$ eV colored by spin polarization. (d), (e) Same as (b), (c) but colored by sublattice weight. (f) Dispersion along high symmetry path colored by sublattice weight. (g) Density of states for the bands shown in (f).

origin and at an *A* sublattice site with the Hamiltonian $\mathcal{H}_\mathrm{imp} = \sum_i V_\mathrm{imp} \frac{1}{2}(\tau_0 + \tau_z)\delta_{i,0}\sigma_0$ [26]. The full Green's function in real space is given by

$$\mathcal{G}(\mathbf{r}, \mathbf{r}', \omega) = \mathcal{G}^0(\mathbf{r} - \mathbf{r}', \omega) + \mathcal{G}^0(\mathbf{r}, \omega)T(\omega)\mathcal{G}^0(-\mathbf{r}', \omega), \tag{6}$$

where $\mathbf{r}$ denotes unit cell positions and all quantities are matrices in spin- and sublattice space. The T matrix

$$T(\omega) = [1 - \mathcal{H}_\mathrm{imp}\mathcal{G}^0(0, \omega)]^{-1}\mathcal{H}_\mathrm{imp} \tag{7}$$

encompasses scatterings off the impurity. Both the bare Green's function $\mathcal{G}^0_\sigma(\mathbf{r}, \omega)$ and the scattering potential $\mathcal{H}_\mathrm{imp}$, and hence also the T matrix, are diagonal in spin, so we can treat the equations for $\sigma = \uparrow, \downarrow$ independently. The bare Green's function in sublattice space for spin σ reads

$$\left(\mathcal{G}^0_\sigma(\mathbf{k})\right)_{ab} = \sum_\beta \frac{(U_{\sigma,\mathbf{k}})_{a\beta}(U^*_{\sigma,\mathbf{k}})_{b\beta}}{\omega + i\eta - E^\beta_{\sigma,\mathbf{k}}}. \tag{8}$$

The real-space expressions are obtained by Fourier transform, $\mathcal{G}^0_\sigma(\mathbf{r}, \omega) = \sum_\mathbf{k} e^{-i\mathbf{k}\cdot\mathbf{r}}\mathcal{G}^0_\sigma(\mathbf{k})$. This approach is applied to tight-binding models describing *d*-wave and *g*-wave altermagnets on a square lattice. For the particular choice of t_x used here, this applies to the following space groups and Wyckoff positions: SG 14 (2*a*-2*d*), SG 55 (2*a*-2*d*), SG 83 (2*e*-2*f*), SG 123 (2*e*-2*f*), and SG 127 (2*a*-2*d*). The associated band structure, Fermi surface (FS), and density of states (DOS) are summarized for this concrete example in Fig. 1. Parameters for the tight-binding model are given in Appendix A.

The spin-resolved LDOS at position $\mathbf{r}$ is obtained from $\rho_\sigma(\mathbf{r}, \omega) = -\frac{1}{\pi}\mathrm{Im}\mathcal{G}_\sigma(\mathbf{r}, \mathbf{r}, \omega)$ and the homogeneous DOS far away from the impurity is given by $\rho^0_\sigma(\omega) = -\frac{1}{\pi}\mathrm{Im}\mathcal{G}^0_\sigma(0, \omega)$ [27]. We define the inhomogeneous part of the LDOS by subtracting the DOS far away from the impurity as $\delta\rho_\sigma(\mathbf{r}, \omega) = \rho_\sigma(\mathbf{r}, \omega) - \rho^0_\sigma(\omega)$.

To quantify the symmetry breaking in the LDOS, we further define

$$\delta\rho_{\sigma,\mathrm{asym}}(\mathbf{r}, \omega) = \delta\rho_\sigma(\mathbf{r}, \omega) - \delta\rho_\sigma(\mathcal{S}\mathbf{r}, \omega), \tag{9}$$

where $\mathcal{S}$ is a symmetry operation that relates the altermagnetic hopping parameters of the two sublattices. For a *d*-wave altermagnet as shown in Fig. 1(a), this corresponds to a C_4 rotation or a mirror operation M_x or M_y along the lattice vectors. For a planar *g*-wave altermagnet, $\mathcal{S}$ is a mirror operation M_x, M_y or along the diagonals M_d, $M_{d'}$. The spin-summed LDOS is $\rho = \sum_\sigma \rho_\sigma$ and all derived spin-summed quantities are calculated accordingly.

B. Self-consistent real-space formulation

A limitation of the T-matrix method is that it depends on the bare Green's function of the homogeneous lattice and feedback effects due to the impurity potential close to the disorder site are not taken into account. To include effects from density modulations in the vicinity of the impurity at the mean-field level, we additionally solve the impurity problem starting from a real-space Hamiltonian $\mathcal{H}$ defined on an $N \times N$ grid with periodic boundary conditions using the same hopping integrals and parameters as before. Instead of fixing a global value for the order parameter N, we obtain it self-consistently by adding an on-site interaction term to the Hamiltonian $\mathcal{H} = \mathcal{H}_0 + \mathcal{H}_\mathrm{imp} + \mathcal{H}_\mathrm{int}$ for each lattice site individually [16]. The on-site Hubbard U is added to the model and we perform a mean-field decoupling

$$\begin{aligned}\mathcal{H}_\mathrm{int}(\mathbf{r}_i) &= U n_{i\uparrow}n_{i\downarrow} \\ &\approx \sum_\sigma \frac{U}{2}\big(\langle n_i\rangle - \sigma N_i\big)n_{i\sigma} - U\langle n_{i\downarrow}\rangle\langle n_{i\uparrow}\rangle,\end{aligned} \tag{10}$$

where $\langle n_i\rangle = \langle n_{i\uparrow} + n_{i\downarrow}\rangle$ denotes the local electron filling and $N_i = \langle n_{i\uparrow} - n_{i\downarrow}\rangle$ the order parameter at site i. We neglect the constant term $U\langle n_{i\downarrow}\rangle\langle n_{i\uparrow}\rangle$ and absorb the term $\frac{U}{2}\langle n_0\rangle$ containing the average filling $\langle n_0\rangle$ into the chemical potential and keep $\langle \delta n_i\rangle = \langle n_i\rangle - \langle n_0\rangle$ for the self-consistency equation, so the interacting part of the Hamiltonian becomes in mean-field

approximation

$$\mathcal{H}_{\mathrm{MF,int}}(\mathbf{r}_i) = \sum_{\sigma} \frac{U}{2}\big(\langle \delta n_i \rangle - \sigma N_i\big) n_{i\sigma}. \tag{11}$$

We solve the resulting Hamiltonian $\mathcal{H} = \mathcal{H}_0 + \mathcal{H}_{\mathrm{imp}} + \mathcal{H}_{\mathrm{MF,int}}$ by numerical diagonalization, use the eigenvalues and eigenvectors to calculate the mean fields $\langle n_i \rangle$ and N_i as thermal averages at temperature $T = 0.01$ eV at fixed filling, i.e., $\sum_i \langle \delta n_i \rangle = 0$, and iterate until convergence. Afterwards, we use the eigenvalues and eigenvectors again to obtain the spatially resolved Green's function and the associated LDOS.

III. RESULTS

A. Signatures from altermagnetic minimal model

We first apply the T-matrix formalism described above to a minimal model example featuring d-wave spin splitting $t_z = 4t_4 \sin k_x \sin k_y$. In Fig. 2(a) we show the calculated LDOS at representative sites close to an impurity with repulsive potential of $V_{\mathrm{imp}} = 1.8$ eV. The nonmagnetic impurity induces a symmetry breaking of the LDOS close to the disorder site as seen by the splitting of the results on the sites of the same color [inset of Fig. 2(a)], which are connected by a 90° rotation (full line, dashed). This signature is present at all energies and is not qualitatively affected by the choice of impurity potential. Far away from the impurity, the DOS will converge to the bulk DOS shown in Fig. 1(g). For further analysis and presentation of LDOS maps, we choose a probe energy of $\omega = 0.15$ eV as there the symmetry breaking is rather large. However, the symmetry statements are valid across all energies. Importantly, breaking of C_4 symmetry is not only present in the spin-resolved LDOS evident from Figs. 2(d)–2(g), but also in the total LDOS as seen from Figs. 2(b) and 2(c). As seen from Figs. 2(c), 2(e) and 2(f) the symmetry and the nodal lines of the d-wave altermagnet are directly imprinted in the total LDOS where $\delta\rho_{\mathrm{asym}}$ vanishes. In this respect, local nonmagnetic disorder acts as a local signature of the underlying altermagnetic order. For disorder located on the B sublattice sites, the resulting LDOS is identical to those presented in Fig. 2 upon a C_4 rotation and exchange of spin component. d-wave altermagnets with $t_z = t_4(\cos k_x - \cos k_y)$ spin splitting can be obtained from models classified by layer groups L61 and a special case of L51 (see Table II), but are not further discussed here. In this case, the imprinted nodal lines will be 45° rotated compared to the d-wave case discussed above. The resulting LDOS impurity effect is also calculated for a g-wave altermagnet where the parameters from Table I are used together with $t_z = t_4 \sin k_x \sin k_y(\cos k_x - \cos k_y)$. Figure 3(a) shows the DOS modulations in this g-wave altermagnet. From $\delta\rho_{\mathrm{asym}}$ as seen in Fig. 3(b) it is evident that there is no effect along the horizontal, vertical, and diagonal directions which imprints the nodal lines of the g-wave spin splitting. The spin-up and spin-down DOS are not equally affected by the impurity and their contributions to the total LDOS can interfere constructively or destructively for different sites, meaning the pattern of the $\delta\rho_\sigma$ is different, but they break the same symmetry. For the particular choice of ω and V_{imp}, the breaking of the LDOS is strongest for spin down [see Figs. 2(g) and 3(f)].

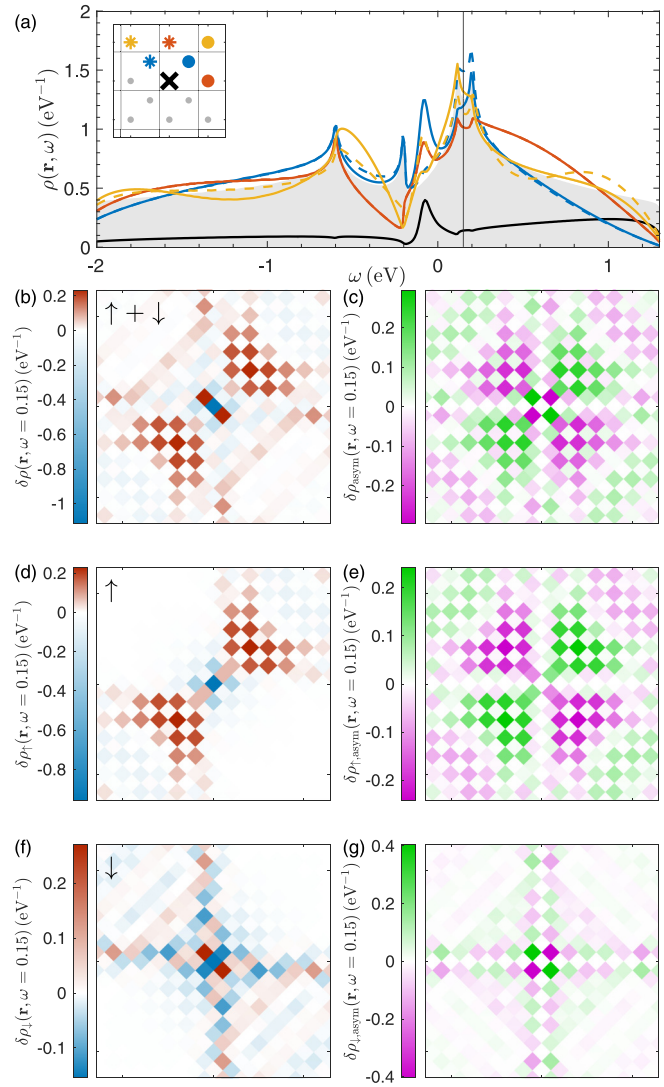

FIG. 2. (a) LDOS as a function of energy in the vicinity of a nonmagnetic impurity with $V_{\mathrm{imp}} = 1.8$ eV. The colored circles (stars) in the inset indicate the site of the corresponding solid (dashed) line. Same colored sites are related by 90° rotation around the impurity. The homogeneous DOS far away from the impurity is shown in gray and the line at $\omega = 0.15$ eV indicates the energy chosen in panels (b)–(g). (b), (d), (f) LDOS without homogeneous background in real-space summed over both spins and for spin-up and spin-down electrons, respectively. (c), (e), (g) Difference of the LDOS and 90° rotated LDOS. Calculations are done with a grid size of 512×512 k points at $\eta = 5$ meV.

In all cases, nonmagnetic impurities uncover not only the presence of altermagnetism but also indicate the underlying altermagnetic order itself. The LDOS pattern for an impurity on a B or A sublattice is related by the same symmetry operation as the sublattices A and B themselves, i.e., an exchange of the spins combined with a C_4 rotation for the d-wave case and a mirror symmetry for the g-wave case.

B. Altermagnet with vanishing order parameter

Is the impurity-induced symmetry breaking exclusive to the magnetic state or can it also manifest in the absence of magnetism? To examine this question, we study the case of

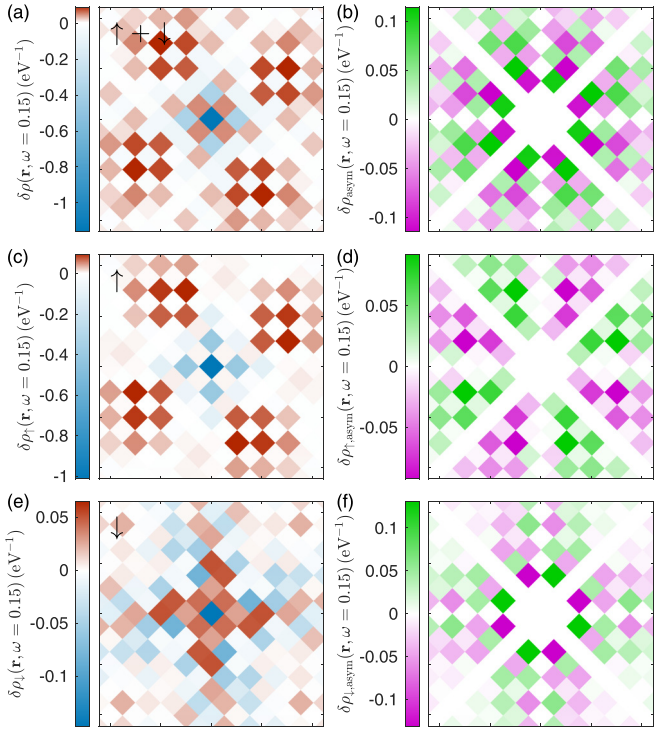

FIG. 3. (a), (c), (e) LDOS without homogeneous background for an altermagnet with g-wave splitting spin summed and spin resolved for spin-up and spin-down, respectively. (b) Difference of the LDOS and LDOS mirrored along one of the g-wave nodal lines of the left column figures.

vanishing order parameter $N = 0$ and keep the t_z term in the tight-binding model since it is generated by the local environments of the atoms of the sublattice. Note that the eigenenergies will be spin degenerate in this case and there are no spin split bands. Yet the LDOS in Fig. 4(a) shows again breaking of C_4 symmetry but $\delta\rho_{\text{asym}}$ is finite only on the sites of the same sublattice as the impurity and zero on all sites of the opposite sublattice sites, apparent in the checkerboard pattern in Fig. 4(b).

We sketch an explanation as follows. Each scattering process of an electron on a B sublattice site with the impurity on the A sublattice must involve an odd number of intersublattice hopping processes $t_{A\leftrightarrow B}$, given by the t_x term. Scattering processes including t_z can potentially be symmetry breaking. While t_z commutes with intrasublattice hoppings, we note that they anticommute with intersublattice hoppings, meaning $t_{A\leftrightarrow B}t_z = -t_z t_{A\leftrightarrow B}$. When summing over all possible scattering processes, this fact together with the odd number of sublattice changes makes all terms containing t_z cancel and hence the LDOS on the B sublattice does not break any of the point group symmetries. For scattering processes between the impurity and an A sublattice site there is an even number of hopping processes that change the sublattice and we observe symmetry breaking as shown in Fig. 4(b). This argument is based on the fact that we assume hoppings to be homogeneous regardless of the impurity site and the T-matrix formalism considers the homogeneous, bare Green's function. In reality, the presence of an impurity strongly affects hopping processes in its vicinity.

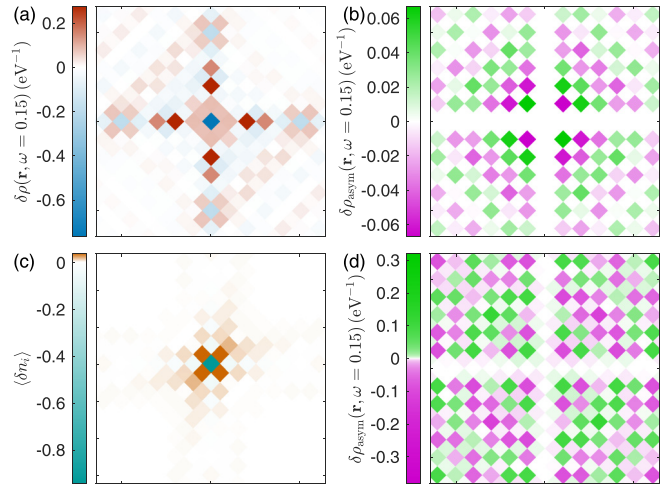

FIG. 4. (a) LDOS from a T-matrix calculation without homogeneous background for an altermagnet in the NS (i. e., $N = 0$) in real space and (b) LDOS asymmetry with a signal only on the A sublattice. (c) Deviation of electron density from self-consistent mean-field calculation with 64×64 elementary cells and $U = 0.9$ eV and (d) resulting asymmetric part of the LDOS. The color bar in (d) is logarithmic to accentuate the small values on the B sublattice.

To take this into account and study its effect, we consider the system in real space and calculate the order parameter self-consistently. Treating the order parameter on a mean-field level gives a magnetic transition at $U \approx 0.95$ eV. For $U = 0.9$ eV the system is in the nonmagnetic normal state and the self-consistent order parameter is numerically zero, yet the electron density shifts close to the impurity and breaks C_4 symmetry as shown in Fig. 4(c). Calculating the Green's function from this real space Hamiltonian via exact diagonalization now reveals symmetry breaking of the LDOS on both sublattices, but the effect is still more than one order of magnitude smaller on the B sublattice; see Fig. 4(d).

Consequently, a symmetry-broken LDOS close to an impurity site is not sufficient to indicate altermagnetism, as it can also occur in the nonmagnetic state. Additionally, Néel order must be shown by experimental techniques like neutron scattering to have conclusive evidence of altermagnetism. In addition, even in the absence of magnetism, symmetry breaking of the LDOS indicates the presence and strength of the altermagnetic hopping t_z which induces the spin splitting once the material becomes magnetic at lower temperatures or by doping.

In the normal state close to the transition, magnetic disorder can induce altermagnetic order locally. For some systems, it is well known that nonmagnetic impurities can also pin local regions of the low-temperature ordered phase [28–35]. For the present model for altermagnetism, however, we have not found evidence for this effect.

C. Impurity response from one-band model

A frequently used model for altermagnetic metals in the literature reduces complexity by applying a one-band model formulated in band space. Instead of exhibiting a sublattice degree of freedom, it is assumed that only a single band

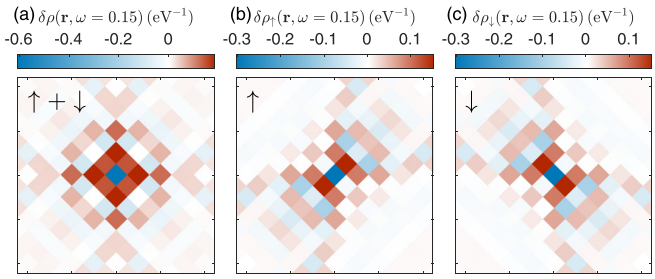

FIG. 5. (a) Spin-summed and (b),(c) spin-resolved LDOS for a nonmagnetic impurity in the one-band model, Eq. (12). The symmetry breaking occurs in each of the spin channels separately, but cancels in the total spin-summed LDOS in contrast to models built on the sublattice degrees of freedom; see Figs. 2 and 3.

crosses the Fermi level and that it exhibits a momentum-dependent spin splitting as recently classified and expressed in an effective momentum-dependent magnetic field [36]. In this case the Hamiltonian is of the form

$$\mathcal{H}_{1\mathrm{SL}} = \varepsilon_{0,\mathbf{k}}\sigma_0 + Nt_{z,\mathbf{k}}\sigma_z. \tag{12}$$

The specific terms and tight-binding parameters are listed in Appendix A. In this subsection we study the local impurity-induced signatures obtained within such a one-band model and compare them to the results obtained within the minimal models based on sublattice site symmetries. Due to the lack of sublattice degree of freedom, the form of the potential scatterer for this model is $\mathcal{H}_{\mathrm{imp}} = \sum_i V_{\mathrm{imp}}\delta_{i,0}\sigma_0$. The main distinction between the two models can be inferred from Fig. 5. For an example case of d-wave spin splitting, it is observed that the symmetry is broken only in the separate spin channels, as seen from Figs. 5(b) and 5(c), and that they cancel in the spin-summed LDOS as evident from Fig. 5(a). This highlights a fundamental difference compared to results obtained from models based on the underlying sublattice degree of freedom. In addition, in the normal state, i.e., without Néel order and spin-split bands, there cannot be a symmetry breaking from the impurity within the one-band model, in contrast to the results of Fig. 4.

D. Quasiparticle interference

The same arguments hold for quasiparticle interference (QPI) in altermagnets: while one-band models produce anisotropy only in the spin-split LDOS response [24,25], models that are based on the sublattice degrees of freedom will feature spatial anisotropy already in the total LDOS. Intuitively, this can be seen directly from Figs. 1(d) and 1(e) highlighting the sublattice character of the states at the Fermi level.

To sustain this argument, we calculate the QPI spectra by Fourier transforming the LDOS and omit the translation invariant term in Eq. (6), as it only contributes to a Bragg peak at $\mathbf{q} = 0$. The density modulations in momentum space read

$$\delta\rho(\mathbf{q},\omega) = -\frac{1}{\pi}\sum_{\mathbf{r}} e^{-i\mathbf{q}\cdot\mathbf{r}}\mathrm{Im}[\mathcal{G}^0(\mathbf{r},\omega)T(\omega)\mathcal{G}^0(-\mathbf{r},\omega)]. \tag{13}$$

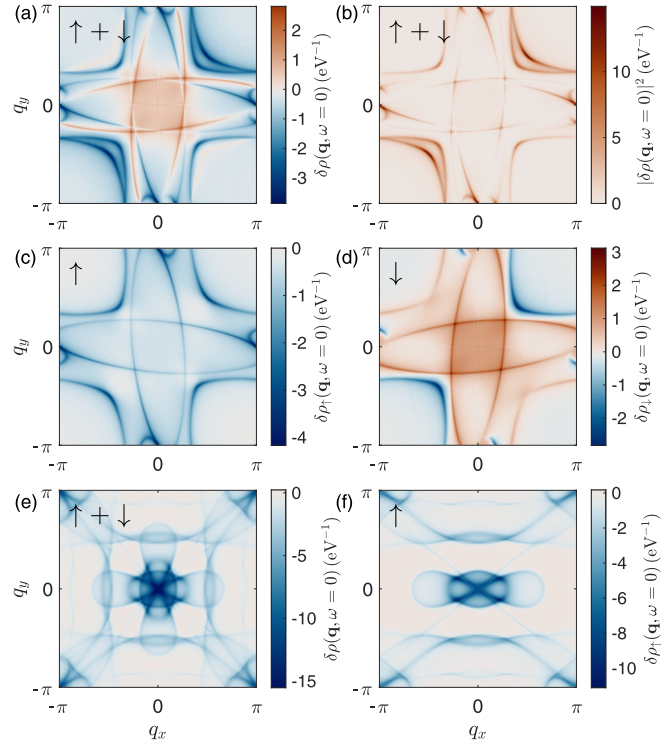

FIG. 6. (a) Spin-summed QPI spectrum for an impurity in a two-band d-wave altermagnet. (b) Power spectrum of panel (a) as measured in experiments. (c),(d) Spin-resolved QPI spectra of panel (a). (e) Spin-summed QPI spectrum in the single-band model and (f) spin-resolved QPI spectum showing only the spin up contribution in panel (e). We use 301 × 301 unit cells for the calculation of the spectra.

We present the QPI spectra at $\omega = 0$ of a d-wave altermagnet for the model including a sublattice degree of freedom [Eq. (2)] and the single-band model [Eq. (12)] in Fig. 6. Again, a symmetry breaking can be observed already in the spin-summed spectrum for the two-band model as seen in Figs. 6(a)–6(d), whereas for the single-band model the symmetry is broken only in the spin-resolved spectrum as shown in Figs. 6(e) and 6(f), since the spectra for the spin up and down channels are related by a 90° rotation. For better comparability to scanning tunneling conductance experiments, we also show the calculated power spectrum as the amplitude squared of the QPI signal in Fig. 6(b) for the two-band model. Furthermore, the spectra for impurities on opposite sublattices are symmetry related [here a C_4 rotation of Figs. 6(a) and 6(b)]. We point out that symmetry breaking effects average out for large scanning areas for similar distribution of impurities on the sublattices. To detect the symmetry breaking, it might be needed to examine small fields of view with imbalanced number of impurities on the two sublattices or experimentally assign the impurities to the sublattices and selectively perform the Fourier transformation as presented in Ref. [37].

E. Interplay with superconductivity

The effect of impurities in gapped systems can lead to very sharp impurity bound states as exemplified by sharp impurity resonances at low energies in superconductors, which can

be used to amplify signatures of underlying ordered states [37–39]. We therefore incorporate superconductivity from an altermagnetic metallic phase [40], e.g., by proximity effect or intrinsic Cooper pairing instability by use of the Nambu formalism. We aim to include only spin-singlet superconductivity, allowing us to decompose the Bogoliubov–de Gennes (BdG) Hamiltonian with sublattice, spin, and Nambu degrees of freedom into two 4×4 blocks

$$\mathcal{H}_{\mathrm{BdG}} = \begin{pmatrix} \mathcal{H}_{\uparrow,\mathbf{k}} & \Delta_{\mathbf{k}} \\ \Delta_{\mathbf{k}}^{\dagger} & -\mathcal{H}_{\downarrow,-\mathbf{k}}^{T} \end{pmatrix}, \tag{14}$$

in the Nambu spinor basis $\Psi_{\mathbf{k}}^{\dagger} = (c_{\uparrow\mathbf{k}}^{A\dagger}, c_{\uparrow\mathbf{k}}^{B\dagger}, c_{\downarrow-\mathbf{k}}^{A}, c_{\downarrow-\mathbf{k}}^{B})$. Here, we write the BdG Hamiltonian for spin up electrons and spin down holes. The second, equivalent block of the BdG Hamiltonian is obtained by reversing the spins. For the SC gap, we consider a simple constant order parameter in band space $\Delta_{\mathrm{b}} = \Delta\mathbb{1}$. Using the unitary transformation Eq. (3) of the normal state, we back transform Δ_{b} and obtain the corresponding order parameter $\Delta_{\mathbf{k}}$ in sublattice space

$$\Delta_{\mathbf{k}} = U_{\uparrow,\mathbf{k}} \Delta_{\mathrm{b}} U_{\downarrow,-\mathbf{k}}^{T}, \tag{15}$$

which becomes momentum dependent and can be used for input to Eq. (14). The band gap edge and the coherence peak shift approximately linear with the maximum of t_z at the Fermi level. When the altermagnetic order parameter becomes large, the gap eventually closes and the superconducting state features a Bogoliubov Fermi surface [41] as generically expected in superconductors with broken time-reversal symmetry [42,43]. Using the expression Eq. (15) within the T-matrix approach, in-gap bound states are found where the real part of the T-matrix in Eq. (7) exhibits poles. The nonmagnetic impurity potential in the Nambu spinor basis is $\mathcal{H}_{\mathrm{imp}} = V_{\mathrm{imp}} \frac{1}{2}(\tau_0 + \tau_z)\sigma_z$ [44]. We solve for the real roots of the T-matrix to calculate the bound state energy ω_{bs} for a range of impurity potentials at a chemical potential $\mu = 0.3$ eV. Examining the result in Fig. 7(a), one sees that the altermagnetic order allows for the existence of in-gap bound states despite the nonmagnetic nature of the impurities [22]. The corresponding LDOS as calculated from the T-matrix approach exhibits pairs of sharp peaks at $\pm\omega_{\mathrm{bs}}$ in the gapped region; see Fig. 7(b). We note, however, that the in-gap bound states are not guaranteed by symmetry and depend on the dispersion and chemical potential. In the nonmagnetic state, the transformation in Eq. (15) becomes trivial with $\Delta_{\mathbf{k}} = \Delta_{\mathrm{b}}$ and no bound states are observed. At the bound state energies, the disorder-induced symmetry breaking of the LDOS is strongly enhanced as evident from Figs. 7(c) and 7(d), making proximity-induced superconductivity in altermagnets an interesting platform to detect local signatures of altermagnetism.

IV. CONCLUSIONS

We have used microscopic models for altermagnetic materials based on the relationship between the site symmetry of magnetic atoms and the point group symmetry of the associated space group, in order to study their real-space fingerprints in terms of the modified local density of states near impurity sites. We found the momentum structure of the spin-dependent band splitting to be directly imprinted on the total LDOS around the impurity site. This finding suggests that scanning tunneling conductance experiments can be used to detect altermagnets, a property that may be particularly useful in materials where domains average out the generic properties of altermagnets. Furthermore, we demonstrate that the lower site symmetry is imprinted on impurity states already without magnetic order, whereas screening from the itinerant electrons makes this signal very weak. Gapping of the electronic structure allows for sharp impurity bound states such that already conventional superconductivity can easily induce low-energy bound states from potential scatterers.

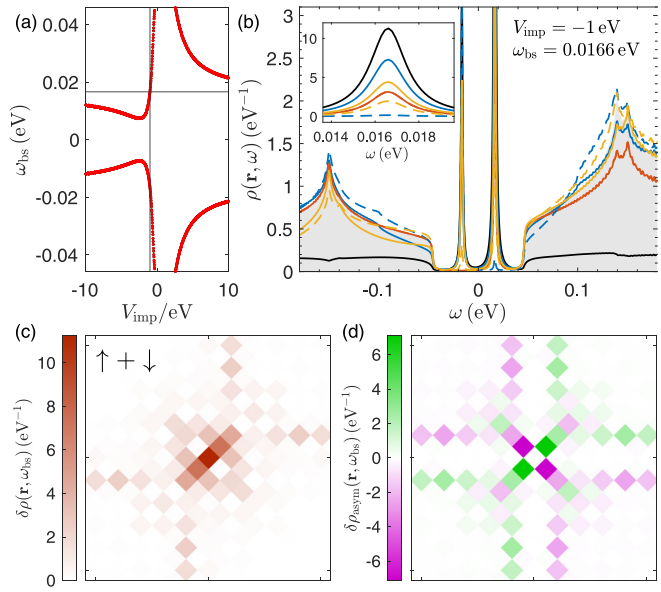

FIG. 7. (a) Bound state energy as function of impurity potential; the vertical and horizontal line indicate the impurity potential and corresponding bound state energy used for the other panels. (b) LDOS at lattice sites close to the impurity; the same colored sites are related by 90° rotation with the same color code as in 2(a). The inset shows magnification near the bound state energy $\omega_{\mathrm{bs}} = 16.6$ meV at $V_{\mathrm{imp}} = -1$ eV, both indicated by lines in panel (a). (c), (d) LDOS and asymmetric part of the LDOS at ω_{bs}, respectively. Calculations are done with a grid size of 1024×1024 k points at $\eta = 1$ meV.

ACKNOWLEDGMENTS

J.G. acknowledges support from the Independent Research Fund Denmark, Grant No. 3103-00008B. A.K. acknowledges support by the Danish National Committee for Research Infrastructure (NUFI) through the ESS-Lighthouse Q-MAT. D.F.A. was supported by National Science Foundation Grant No. DMREF 2323857. Work at UWM was also supported by a grant from the Simons Foundation (No. SFI-MPS-NFS-00006741-02, M.R. and Y.Y.).

DATA AVAILABILITY

The data that support the findings of this article are not publicly available upon publication because it is not technically feasible and/or the cost of preparing, depositing, and hosting the data would be prohibitive within the terms of this

TABLE I. Hopping parameters for the minimal model [see Eq. (2)] in eV.

t_1	t_2	t_3	t_4	μ	N
0.425	0.05	−0.025	−0.075	0.3	0.2

research project. The data are available from the authors upon reasonable request.

APPENDIX A: TIGHT-BINDING PARAMETERS

The terms in the tight-binding Hamiltonian (2) are given by

$$\varepsilon_0 = -2t_2(\cos k_x + \cos k_y) - 4t_3 \cos k_x \cos k_y - \mu, \quad \text{(A1)}$$

$$t_x = -t_1(1 + e^{-ik_x} + e^{-ik_y} + e^{-i(k_x+k_y)})$$
$$= -4t_1 e^{-i(\frac{k_x}{2}+\frac{k_y}{2})} \cos\frac{k_x}{2} \cos\frac{k_y}{2}, \quad \text{(A2)}$$

$$t_z = 4t_4 \sin k_x \sin k_y, \quad \text{(A3)}$$

as illustrated in Fig. 1. The values of the hopping parameters are given in Table I and chosen the same as in the 2D model from Ref. [16].

For the single band Hamiltonian in Eq. (12), the terms are given by

$$\varepsilon_0 = -2t_1(\cos k_x + \cos k_y) - 4t_2 \cos k_x \cos k_y$$
$$- 2t_3(\cos 2k_x + \cos 2k_y) - \mu, \quad \text{(A4)}$$

$$Nt_z = 4t_4 \sin k_x \sin k_y, \quad \text{(A5)}$$

with parameters specified in Table I. Note that the BZ is different from the one of Eq. (2) since there is only one site per unit cell.

TABLE II. Tight-binding coefficients for 2D layer groups and Wyckoff positions with two atoms per unit cell at the inversion center. Abbreviation $c_i \equiv \cos k_i$, $s_i \equiv \sin k_i$, $c_{i/2} \equiv \cos\frac{k_i}{2}$, and $s_{i/2} \equiv \sin\frac{k_i}{2}$ applies. Altermagnets with d-wave spin-splitting can be found in L15, L16, L17, L40, L44, L51, L61, and L63, while g-wave altermagnets can be found in L63. Coefficients are omitted for simplicity. We have included entries which are 0 in the τ_z column. These entries have magnetic ground states that can be classified as altermagnetic, but exhibit no spin-splitting.

2D layer groups	Wyckoff positions	τ_x	τ_z
L7 ($p112/a$)	2a-2b	$c_{x/2}$	0
L15 ($p2_1/m11$)	2a-2b	$c_{x/2}$	$s_x s_y$
L16 ($p2/b11$)	2a-2b	$c_{y/2}$	$s_x s_y$
L17 ($p2_1/b11$)	2a-2b	$c_{x/2}c_{y/2}$	$s_x s_y$
L38 ($pmaa$)	2a-2b	$c_{x/2}$	0
L40 ($pmam$)	2a-2b	$c_{x/2}$	$s_x s_y$
L41 ($pmma$)	2a-2b	$c_{x/2}$	0
L42 ($pman$)	2a-2b	$c_{x/2}c_{y/2}$	0
L44 ($pbam$)	2a-2b	$c_{x/2}c_{y/2}$	$s_x s_y$
L51 ($p4/m$)	2c	$c_{x/2}c_{y/2}$	$t_{z1}(c_x - c_y) + t_{z2} s_x s_y$
L61 ($p4/mmm$)	2c	$c_{x/2}c_{y/2}$	$c_x - c_y$
L63 ($p4/mbm$)	2a	$c_{x/2}c_{y/2}$	$s_x s_y (c_x - c_y)$
L63 ($p4/mbm$)	2b	$c_{x/2}c_{y/2}$	$s_x s_y$

APPENDIX B: TWO-DIMENSIONAL LAYER GROUPS

For numerical calculations, 2D minimal models are useful. Using our earlier approach for developing minimal models [16], we have developed 2D layer group-based minimal models. These models are written in Table II for all 2D layer groups that have a primitive lattice and also have Wyckoff positions of order 2 that contain inversion in the Wyckoff site symmetry group.

[1] L. Šmejkal, J. Sinova, and T. Jungwirth, Emerging research landscape of altermagnetism, Phys. Rev. X **12**, 040501 (2022).

[2] L. Šmejkal, J. Sinova, and T. Jungwirth, Beyond conventional ferromagnetism and antiferromagnetism: A phase with nonrelativistic spin and crystal rotation symmetry, Phys. Rev. X **12**, 031042 (2022).

[3] S. Reimers, L. Odenbreit, L. Šmejkal, V. N. Strocov, P. Constantinou, A. B. Hellenes, R. Jaeschke Ubiergo, W. H. Campos, V. K. Bharadwaj, A. Chakraborty, T. Denneulin, W. Shi, R. E. Dunin-Borkowski, S. Das, M. Kläui, J. Sinova, and M. Jourdan, Direct observation of altermagnetic band splitting in CrSb thin films, Nat. Commun. **15**, 2116 (2024).

[4] J. Ding, Z. Jiang, X. Chen, Z. Tao, Z. Liu, T. Li, J. Liu, J. Sun, J. Cheng, J. Liu, Y. Yang, R. Zhang, L. Deng, W. Jing, Y. Huang, Y. Shi, M. Ye, S. Qiao, Y. Wang, Y. Guo *et al.*, Large band splitting in g-wave altermagnet CrSb, Phys. Rev. Lett. **133**, 206401 (2024).

[5] J. Krempaský, L. Šmejkal, S. W. D'Souza, M. Hajlaoui, G. Springholz, K. Uhlířová, F. Alarab, P. C. Constantinou, V. Strocov, D. Usanov, W. R. Pudelko, R. González-Hernández, A. B. Hellenes, Z. Jansa, H. Reichlová, Z. Šobáň, R. D. Gonzalez Betancourt, P. Wadley, J. Sinova, D. Kriegner *et al.*, Altermagnetic lifting of Kramers spin degeneracy, Nature (London) **626**, 517 (2024).

[6] S. Lee, S. Lee, S. Jung, J. Jung, D. Kim, Y. Lee, B. Seok, J. Kim, B. G. Park, L. Šmejkal, C.-J. Kang, and C. Kim, Broken Kramers degeneracy in altermagnetic MnTe, Phys. Rev. Lett. **132**, 036702 (2024).

[7] T. Osumi, S. Souma, T. Aoyama, K. Yamauchi, A. Honma, K. Nakayama, T. Takahashi, K. Ohgushi, and T. Sato, Observation of a giant band splitting in altermagnetic MnTe, Phys. Rev. B **109**, 115102 (2024).

[8] O. Fedchenko, J. Minr, A. Akashdeep, S. W. D'Souza, D. Vasilyev, O. Tkach, L. Odenbreit, Q. Nguyen, D. Kutnyakhov, N. Wind, L. Wenthaus, M. Scholz, K. Rossnagel, M. Hoesch, M. Aeschlimann, B. Stadtmüller, M. Kläui, G. Schönhense, T. Jungwirth, A. B. Hellenes *et al.*, Observation of time-reversal symmetry breaking in the band structure of altermagnetic RuO_2, Sci. Adv. **10**, eadj4883 (2024).

[9] H.-Y. Ma, M. Hu, N. Li, J. Liu, W. Yao, J.-F. Jia, and J. Liu, Multifunctional antiferromagnetic materials with giant piezomagnetism and noncollinear spin current, Nat. Commun. **12**, 2846 (2021).

[10] S. H. Pan, E. W. Hudson, K. M. Lang, H. Eisaki, S. Uchida, and J. C. Davis, Imaging the effects of individual zinc impurity atoms on superconductivity in $Bi_2Sr_2CaCu_2O_{8+\delta}$, Nature (London) **403**, 746 (2000).

[11] E. W. Hudson, K. M. Lang, V. Madhavan, S. H. Pan, H. Eisaki, S. Uchida, and J. C. Davis, Interplay of magnetism and high-T_c superconductivity at individual Ni impurity atoms in $Bi_2Sr_2CaCu_2O_{8+\delta}$, Nature (London) **411**, 920 (2001).

[12] A. V. Balatsky, I. Vekhter, and J.-X. Zhu, Impurity-induced states in conventional and unconventional superconductors, Rev. Mod. Phys. **78**, 373 (2006).

[13] A. Kreisel, P. Choubey, T. Berlijn, W. Ku, B. M. Andersen, and P. J. Hirschfeld, Interpretation of scanning tunneling quasiparticle interference and impurity states in cuprates, Phys. Rev. Lett. **114**, 217002 (2015).

[14] S. Chi, R. Aluru, U. R. Singh, R. Liang, W. N. Hardy, D. A. Bonn, A. Kreisel, B. M. Andersen, R. Nelson, T. Berlijn, W. Ku, P. J. Hirschfeld, and P. Wahl, Impact of iron-site defects on superconductivity in LiFeAs, Phys. Rev. B **94**, 134515 (2016).

[15] P. Choubey, A. Kreisel, T. Berlijn, B. M. Andersen, and P. J. Hirschfeld, Universality of scanning tunneling microscopy in cuprate superconductors, Phys. Rev. B **96**, 174523 (2017).

[16] M. Roig, A. Kreisel, Y. Yu, B. M. Andersen, and D. F. Agterberg, Minimal models for altermagnetism, Phys. Rev. B **110**, 144412 (2024).

[17] M. Roig, Y. Yu, R. C. Ekman, A. Kreisel, B. M. Andersen, and D. F. Agterberg, Quasi-symmetry constrained spin ferromagnetism in altermagnets, arXiv:2412.09338.

[18] N. Heinsdorf, Altermagnetic instabilities from quantum geometry, Phys. Rev. B **111**, 174407 (2025).

[19] S. Sorn, Antichiral surface states and Su-Schrieffer-Heeger physics in rutile altermagnets, Phys. Rev. B **111**, L161109 (2025).

[20] J. Sødequist and T. Olsen, Two-dimensional altermagnets from high throughput computational screening: Symmetry requirements, chiral magnons, and spin-orbit effects, Appl. Phys. Lett. **124**, 182409 (2024).

[21] D. Zhu, D. Liu, Z.-Y. Zhuang, Z. Wu, and Z. Yan, Field-sensitive dislocation bound states in two-dimensional d-wave altermagnets, Phys. Rev. B **110**, 165141 (2024).

[22] A. Maiani and R. S. Souto, Impurity states in altermagnetic superconductors, arXiv:2409.01008.

[23] P. Sukhachov and J. Linder, Impurity-induced Friedel oscillations in altermagnets and p-wave magnets, Phys. Rev. B **110**, 205114 (2024).

[24] H.-R. Hu, X. Wan, and W. Chen, Quasiparticle interference in altermagnets, Phys. Rev. B **111**, 035132 (2025).

[25] W. Chen, X. Zhou, D. Zhang, Y.-Q. Xu, and W.-K. Lou, Impurity scattering and Friedel oscillations in altermagnets, Phys. Rev. B **110**, 165413 (2024).

[26] In altermagnets, the sublattice sites are related by a proper (or improper) rotation in the normal state and by time reversal and the corresponding proper (or improper) rotation. Thus an impurity on a B sublattice exhibits the same response modulo the rotation operation in the normal state and modulo the rotation and time-reversal operation in the magnetic state.

[27] Note that the position $\mathbf{r}$ refers to a position of a lattice point rather than an elementary cell and the corresponding matrix element of the Green's function is meant on the right-hand side.

[28] Y. Chen and C. S. Ting, States of local moment induced by nonmagnetic impurities in cuprate superconductors, Phys. Rev. Lett. **92**, 077203 (2004).

[29] J. W. Harter, B. M. Andersen, J. Bobroff, M. Gabay, and P. J. Hirschfeld, Antiferromagnetic correlations and impurity broadening of NMR linewidths in cuprate superconductors, Phys. Rev. B **75**, 054520 (2007).

[30] B. M. Andersen, P. J. Hirschfeld, A. P. Kampf, and M. Schmid, Disorder-induced static antiferromagnetism in cuprate superconductors, Phys. Rev. Lett. **99**, 147002 (2007).

[31] B. M. Andersen and P. J. Hirschfeld, Breakdown of universal transport in correlated d-wave superconductors, Phys. Rev. Lett. **100**, 257003 (2008).

[32] M. Schmid, B. M. Andersen, A. P. Kampf, and P. J. Hirschfeld, d-wave superconductivity as a catalyst for antiferromagnetism in underdoped cuprates, New J. Phys. **12**, 053043 (2010).

[33] J. H. J. Martiny, M. N. Gastiasoro, I. Vekhter, and B. M. Andersen, Impurity-induced antiferromagnetic order in Pauli-limited nodal superconductors: Application to heavy-fermion $CeCoIn_5$, Phys. Rev. B **92**, 224510 (2015).

[34] M. N. Gastiasoro, F. Bernardini, and B. M. Andersen, Unconventional disorder effects in correlated superconductors, Phys. Rev. Lett. **117**, 257002 (2016).

[35] J. H. J. Martiny, A. Kreisel, and B. M. Andersen, Theoretical study of impurity-induced magnetism in FeSe, Phys. Rev. B **99**, 014509 (2019).

[36] P. G. Radaelli, Tensorial approach to altermagnetism, Phys. Rev. B **110**, 214428 (2024).

[37] W. Chen, C. N. Breiø, F. Massee, M. P. Allan, C. Petrovic, J. C. S. Davis, P. J. Hirschfeld, B. M. Andersen, and A. Kreisel, Interplay of hidden orbital order and superconductivity in $CeCoIn_5$, Nat. Commun. **14**, 2984 (2023).

[38] M. N. Gastiasoro and B. M. Andersen, Competing magnetic double-Q phases and superconductivity-induced reentrance of C_2 magnetic stripe order in iron pnictides, Phys. Rev. B **92**, 140506(R) (2015).

[39] M. N. Gastiasoro, I. Eremin, R. M. Fernandes, and B. M. Andersen, Scanning tunnelling spectroscopy as a probe of multi-Q magnetic states of itinerant magnets, Nat. Commun. **8**, 14317 (2017).

[40] B. Brekke, A. Brataas, and A. Sudbø, Two-dimensional altermagnets: Superconductivity in a minimal microscopic model, Phys. Rev. B **108**, 224421 (2023).

[41] S. B. Hong, M. J. Park, and K.-M. Kim, Unconventional p-wave and finite-momentum superconductivity induced by altermagnetism through the formation of Bogoliubov Fermi surface, Phys. Rev. B **111**, 054501 (2025).

[42] D. F. Agterberg, P. M. R. Brydon, and C. Timm, Bogoliubov Fermi surfaces in superconductors with broken time-reversal symmetry, Phys. Rev. Lett. **118**, 127001 (2017).

[43] C. Setty, Y. Cao, A. Kreisel, S. Bhattacharyya, and P. J. Hirschfeld, Bogoliubov Fermi surfaces in spin-$\frac{1}{2}$ systems: Model Hamiltonians and experimental consequences, Phys. Rev. B **102**, 064504 (2020).

[44] Note that here σ_z refers to particle-hole space. By choice of the basis for Eq. (14), electrons carry spin up and holes carry spin down.